Editors' Suggestion

Unified and Consistent Structure Growth Measurements from Joint ACT, SPT, and *Planck* CMB Lensing

Frank J. Qu,[1,2,3,*] Fei Ge,[1,2,4,5] W. L. Kimmy Wu,[1,6,5] Irene Abril-Cabezas,[7,3] Mathew S. Madhavacheril,[8] Marius Millea,[4] Zeeshan Ahmed,[1,6] Ethan Anderes,[9] Adam J. Anderson,[10,11,12] Behzad Ansarinejad,[13] Melanie Archipley,[11,12] Zachary Atkins,[14] Lennart Balkenhol,[15] Nicholas Battaglia,[16,17] Karim Benabed,[15] Amy N. Bender,[18,11,12] Bradford A. Benson,[10,11,12] Federico Bianchini,[1,2,6] Lindsey. E. Bleem,[18,11] Boris Bolliet,[19,3] J. Richard Bond,[20] François. R. Bouchet,[15] Lincoln Bryant,[21] Erminia Calabrese,[22] Etienne Camphuis,[15] John E. Carlstrom,[11,21,23,18,12] Julien Carron,[24] Anthony Challinor,[25,3,26] Clarence L. Chang,[18,11,12] Prakrut Chaubal,[13] Geoff Chen,[27] Paul M. Chichura,[23,11] Steve K. Choi,[28] Aman Chokshi,[27] Ti-Lin Chou,[12,11] Anna Coerver,[29] William Coulton,[25,3] Thomas M. Crawford,[11,12] Cail Daley,[30,31] Omar Darwish,[32] Tijmen de Haan,[33] Mark J. Devlin,[34] Karia R. Dibert,[12,11] Matthew A. Dobbs,[35,36] Michael Doohan,[13] Aristide Doussot,[15] Adriaan J. Duivenvoorden,[37] Jo Dunkley,[14,38] Rolando Dunner,[39] Daniel Dutcher,[14] Carmen Embil Villagra,[7,3] Wendy Everett,[40] Gerrit S. Farren,[41,42] Chang Feng,[43] Simone Ferraro,[41,29,42] Kyle R. Ferguson,[44,45] Kyra Fichman,[23,11] Emily Finson,[46] Allen Foster,[14] Patricio A. Gallardo,[47] Silvia Galli,[15] Anne E. Gambrel,[11] Rob W. Gardner,[21] Neil Goeckner-Wald,[2,1] Riccardo Gualtieri,[18,48] Federica Guidi,[15] Sam Guns,[29] Mark Halpern,[49] Nils W. Halverson,[50,51] J. Colin Hill,[52] Matt Hilton,[53,54] Eric Hivon,[15] Gilbert P. Holder,[43] William L. Holzapfel,[29] John C. Hood,[11] Doug Howe,[27] Alec Hryciuk,[23,11] Nicholas Huang,[29] Johannes Hubmayr,[55] Florian Kéruzoré,[18] Ali R. Khalife,[15] Joshua Kim,[8] Lloyd Knox,[4] Milo Korman,[56] Kayla Kornoelje,[12,11] Arthur Kosowsky,[57] Chao-Lin Kuo,[1,2,6] Hidde T. Jense,[22] Adrien La Posta,[58] Kevin Levy,[13] Amy E. Lowitz,[11] Thibaut Louis,[59] Chunyu Lu,[43] Gabriel P. Lynch,[4] Niall MacCrann,[26,3] Abhishek Maniyar,[1,2,6] Emily S. Martsen,[12,11] Jeff McMahon,[60,61,62,63] Felipe Menanteau,[31,64] Joshua Montgomery,[35] Yuka Nakato,[2] Kavilan Moodley,[65,66] Toshiya Namikawa,[7,67,3] Tyler Natoli,[11] Michael D. Niemack,[68,16] Gavin I. Noble,[69] Yuuki Omori,[12,11] Aaron Ouellette,[43] Lyman A. Page,[14] Zhaodi Pan,[18,11,23] Pascal Paschos,[21] Kedar A. Phadke,[31,64] Alexander W. Pollak,[27] Karthik Prabhu,[4] Wei Quan,[18,23,11] Srinivasan Raghunathan,[64] Mahsa Rahimi,[13] Alexandra Rahlin,[12,11] Christian L. Reichardt,[13] Dave Riebel,[27] Maclean Rouble,[35] John E. Ruhl,[56] Emmanuel Schaan,[6,1] Eduardo Schiappucci,[13] Neelima Sehgal,[70] Carlos E. Sierra,[1,6] Aidan Simpson,[12,11] Blake D. Sherwin,[7,3] Cristóbal Sifón,[71] David N. Spergel,[72] Suzanne T. Staggs,[14] Joshua A. Sobrin,[10,11] Antony A. Stark,[73] Judith Stephen,[21] Chris Tandoi,[31] Ben Thorne,[4] Cynthia Trendafilova,[64] Caterina Umilta,[43] Alexander Van Engelen,[74] Joaquin D. Vieira,[31,43,64] Aline Vitrier,[15] Yujie Wan,[31,64] Nathan Whitehorn,[45] Edward J. Wollack,[75] Matthew R. Young,[10,11] and Jessica A. Zebrowski[11,12,10]

(ACT + SPT-3G Collaborations)

[1]*Kavli Institute for Particle Astrophysics and Cosmology, Stanford University, 452 Lomita Mall, Stanford, California 94305, USA*
[2]*Department of Physics, Stanford University, 382 Via Pueblo Mall, Stanford, California 94305, USA*
[3]*Kavli Institute for Cosmology Cambridge, Madingley Road, Cambridge CB3 0HA, United Kingdom*
[4]*Department of Physics and Astronomy, University of California One Shields Avenue, Davis, California 95616, USA*
[5]*Department of Physics, California Institute of Technology, Pasadena, California 91125, USA*
[6]*SLAC National Accelerator Laboratory, 2575 Sand Hill Road, Menlo Park, California 94025, USA*
[7]*DAMTP, Centre for Mathematical Sciences, University of Cambridge, Wilberforce Road, Cambridge CB3 0WA, United Kingdom*
[8]*Department of Physics and Astronomy, University of Pennsylvania, 209 South 33rd Street, Philadelphia, Pennsylvania 19104, USA*
[9]*Department of Statistics, University of California One Shields Avenue, Davis, California 95616, USA*
[10]*Fermi National Accelerator Laboratory, MS209, P.O. Box 500, Batavia, Illinois 60510, USA*
[11]*Kavli Institute for Cosmological Physics, University of Chicago, 5640 South Ellis Avenue, Chicago, Illinois 60637, USA*
[12]*Department of Astronomy and Astrophysics, University of Chicago, 5640 South Ellis Avenue, Chicago, Illinois 60637, USA*
[13]*School of Physics, University of Melbourne, Parkville, Victoria 3010, Australia*
[14]*Joseph Henry Laboratories of Physics, Jadwin Hall, Princeton University, Princeton, New Jersey 08544, USA*
[15]*Sorbonne Université, CNRS, UMR 7095, Institut d'Astrophysique de Paris, 98 bis bd Arago, 75014 Paris, France*
[16]*Department of Astronomy, Cornell University, Ithaca, New York 14853, USA*
[17]*Universite Paris Cite, CNRS, Astroparticule et Cosmologie, F-75013 Paris, France*
[18]*High-Energy Physics Division, Argonne National Laboratory, 9700 South Cass Avenue, Lemont, Illinois 60439, USA*
[19]*Department of Physics, Madingley Road, Cambridge CB3 0HA, United Kingdom*
[20]*Canadian Institute for Theoretical Astrophysics, University of Toronto, Toronto, Ontario Canada M5S 3H8*
[21]*Enrico Fermi Institute, University of Chicago, 5640 South Ellis Avenue, Chicago, Illinois 60637, USA*

[22]School of Physics and Astronomy, Cardiff University, The Parade, Cardiff, Wales CF24 3AA, United Kingdom
[23]Department of Physics, University of Chicago, 5640 South Ellis Avenue, Chicago, Illinois 60637, USA
[24]Université de Genéve, Département de Physique Théorique, 24 Quai Ansermet, CH-1211 Genéve 4, Switzerland
[25]Institute of Astronomy, Madingley Road, Cambridge CB3 0HA, United Kingdom
[26]DAMTP, Centre for Mathematical Sciences, University of Cambridge, Wilberforce Road, Cambridge CB3 OWA, United Kingdom
[27]University of Chicago, 5640 South Ellis Avenue, Chicago, Illinois 60637, USA
[28]Department of Physics and Astronomy, University of California Riverside, California 92521, USA
[29]Department of Physics, University of California Berkeley, California 94720, USA
[30]Université Paris-Saclay, Université Paris Cité, CEA, CNRS, AIM, 91191, Gif-sur-Yvette, France
[31]Department of Astronomy, University of Illinois Urbana-Champaign, 1002 West Green Street, Urbana, Illinois 61801, USA
[32]Université de Genève, Département de Physique Théorique et CAP, 24 quai Ernest-Ansermet, CH-1211 Genève 4, Switzerland
[33]High Energy Accelerator Research Organization (KEK), Tsukuba, Ibaraki 305-0801, Japan
[34]Department of Physics and Astronomy, University of Pennsylvania, 209 South 33rd Street, Philadelphia, Pennsylvania 19104, USA
[35]Department of Physics and McGill Space Institute, McGill University, 3600 Rue University, Montreal, Quebec H3A 2T8, Canada
[36]Canadian Institute for Advanced Research, CIFAR Program in Gravity and the Extreme Universe, Toronto, Ontario M5G 1Z8, Canada
[37]Max-Planck-Institut fur Astrophysik, Karl-Schwarzschild-Straße 1, 85748 Garching, Germany
[38]Department of Astrophysical Sciences, Peyton Hall, Princeton University, Princeton, New Jersey 08544, USA
[39]Instituto de Astrofísica and Centro de Astro-Ingeniería, Facultad de Física, Pontificia Universidad Católica de Chile, Santiago, Chile
[40]Department of Astrophysical and Planetary Sciences, University of Colorado, Boulder, Colorado 80309, USA
[41]Physics Division, Lawrence Berkeley National Laboratory, Berkeley, California 94720, USA
[42]Berkeley Center for Cosmological Physics, University of California Berkeley, California 94720, USA
[43]Department of Physics, University of Illinois Urbana-Champaign, 1110 West Green Street, Urbana, Illinois 61801, USA
[44]Department of Physics and Astronomy, University of California Los Angeles, California 90095, USA
[45]Department of Physics and Astronomy, Michigan State University, East Lansing, Michigan 48824, USA
[46]Physics and Astronomy Department, Stony Brook University, Stony Brook, New York 11794, USA
[47]Department of Physics and Astronomy, University of Pennsylvania, Philadelphia, Pennsylvania 19104, USA
[48]Department of Physics and Astronomy, Northwestern University, 633 Clark St, Evanston, Illinois 60208, USA
[49]Department of Physics and Astronomy, University of British Columbia, Vancouver, British Columbia, Canada
[50]CASA, Department of Astrophysical and Planetary Sciences, University of Colorado, Boulder, Colorado 80309, USA
[51]Department of Physics, University of Colorado, Boulder, Colorado 80309, USA
[52]Department of Physics, Columbia University, New York, New York 10027, USA
[53]Wits Centre for Astrophysics, School of Physics, University of the Witwatersrand, Private Bag 3, 2050, Johannesburg, South Africa
[54]Astrophysics Research Centre, School of Mathematics, Statistics and Computer Science, University of KwaZulu-Natal, Durban 4001, South Africa
[55]Quantum Sensors Division, National Institute of Standards and Technology, 325 Broadway, Boulder, Colorado 80305, USA
[56]Department of Physics, Case Western Reserve University, Cleveland, Ohio 44106, USA
[57]Department of Physics and Astronomy, University of Pittsburgh, Pittsburgh, Pennsylvania 15260, USA
[58]Department of Physics, University of Oxford, Keble Road, Oxford, OX1 3RH, United Kingdom
[59]Université Paris-Saclay, CNRS/IN2P3, IJCLab, 91405 Orsay, France
[60]Kavli Institute for Cosmological Physics, University of Chicago, 5640 South Ellis avenue, Chicago, Illinois 60637, USA
[61]Department of Astronomy and Astrophysics, University of Chicago, 5640 South Ellis avenue, Chicago, Illinois 60637, USA
[62]Department of Physics, University of Chicago, Chicago, Illinois 60637, USA
[63]Enrico Fermi Institute, University of Chicago, Chicago, Illinois 60637, USA
[64]Center for AstroPhysical Surveys, National Center for Supercomputing Applications, Urbana, Illinois 61801, USA
[65]Astrophysics Research Centre, University of KwaZulu-Natal, Westville Campus, Durban 4041, South Africa
[66]School of Mathematics, Statistics and Computer Science, University of KwaZulu-Natal, Westville Campus, Durban 4041, South Africa
[67]Center for Data-Driven Discovery, Kavli IPMU (WPI), UTIAS, The University of Tokyo, Kashiwa, 277-8583, Japan
[68]Department of Physics, Cornell University, Ithaca, New York 14853, USA
[69]Dunlap Institute for Astronomy & Astrophysics and David A. Dunlap Department of Astronomy and Astrophysics, University of Toronto, 50 Saint George Street, Toronto, ON, M5S 3H4, Canada
[70]Physics and Astronomy Department, Stony Brook University, Stony Brook, New York 11794, USA
[71]Instituto de Física, Pontificia Universidad Católica de Valparaíso, Casilla 4059, Valparaíso, Chile
[72]Flatiron Institute, 162 5th Avenue, New York, New York 10010, USA
[73]Center for Astrophysics | Harvard & Smithsonian, 60 Garden Street, Cambridge, Massachusetts 02138, USA
[74]School of Earth and Space Exploration, Arizona State University, Tempe, Arizona 85287, USA
[75]NASA/Goddard Space Flight Center, Greenbelt, Maryland 20771, USA

*Contact author: jq247@cantab.ac.uk

(Received 14 May 2025; revised 6 October 2025; accepted 21 November 2025; published 14 January 2026)

We present the tightest cosmic microwave background (CMB) lensing constraints to date on the growth of structure by combining CMB lensing measurements from the Atacama Cosmology Telescope (ACT), the South Pole Telescope (SPT), and *Planck*. Each of these surveys individually provides lensing measurements with similarly high statistical power, achieving signal-to-noise ratios of approximately 40. The combined lensing band powers represent the most precise CMB lensing power spectrum measurement to date with a signal-to-noise ratio of 61 and an amplitude of $A_{\rm lens}^{\rm recon} = 1.025 \pm 0.017$ with respect to the theory prediction from the best-fit CMB *Planck*-ACT cosmology. The band powers from all three lensing datasets, analyzed jointly, yield a 1.6% measurement of the parameter combination $S_8^{\rm CMBL} \equiv \sigma_8(\Omega_m/0.3)^{0.25} = 0.825^{+0.015}_{-0.013}$. Including dark energy spectroscopic instrument baryon acoustic oscillation (BAO) data improves the constraint on the amplitude of matter fluctuations to $\sigma_8 = 0.829 \pm 0.009$ (a 1.1% determination). When combining with uncalibrated supernovae from `Pantheon+`, we present a 4% sound-horizon-independent estimate of $H_0 = 66.4 \pm 2.5$ km s^{-1} Mpc^{-1}. The joint lensing constraints on structure growth and present-day Hubble rate are fully consistent with a ΛCDM model fit to the primary CMB data from *Planck* and ACT. While the precise upper limit is sensitive to the choice of data and underlying model assumptions, when varying the neutrino mass sum within the ΛCDM cosmological model, the combination of primary CMB, BAO, and CMB lensing drives the probable upper limit for the mass sum towards lower values, comparable to the minimum mass prior required by neutrino oscillation experiments.

DOI: 10.1103/k5yr-3h6d

Introduction—Lensing of the cosmic microwave background (CMB), the deflection of CMB photon paths by intervening large-scale structure, has emerged as a highly robust probe of the mass distribution.

Building on lensing measurements from the satellite-based missions *Wilkinson Microwave Anisotropy Probe* (*WMAP*) [1] and *Planck* [2–4], and from ground-based surveys such as Atacama cosmology telescope (ACT) [5,6] and South Pole telescope (SPT) [7–11], the measurement of CMB lensing has been advanced to the regime of precision cosmology. Notably, direct structure growth measurements via CMB lensing are consistent with the predictions of the ΛCDM model conditioned on the primary CMB measurements [12].

In this Letter, we combine the latest results from *Planck* PR4 [18], ACT DR6 [19–21], and SPT-3G MUSE analysis on the main-field-2-year polarization-only data [[22], SPT-3G M2PM]. These three analyses use data from successively narrower fields and with lower noise levels, yet they achieve comparable lensing power spectrum signal-to-noise ratios. The consistency between these independent measurements, despite their distinct observational strategies, makes their agreement, and consequently the joint constraints presented here, compelling.

We infer the amplitude of structure growth, specifically via a parameter combination of linear matter power fluctuation (σ_8) and the fractional matter energy density (Ω_m), $S_8^{\rm CMBL} \equiv \sigma_8(\Omega_m/0.3)^{0.25}$, which CMB lensing is most sensitive to in the redshift range $z \approx 0.9$–5 and the physical wave number range $k \approx 0.05$–0.3 Mpc^{-1}. This is complementary to the constraints from galaxy surveys [23–31], which are sensitive to lower redshifts and larger k values (smaller physical scales).

We then include baryon acoustic oscillation (BAO) observations, which act as a probe of Ω_m, thereby allowing us to constrain σ_8 separately. We also determine the Hubble constant, H_0, using two approaches: one relying on the sound horizon scale to which BAO is sensitive, and one based on the matter-radiation equality scale to which CMB lensing is sensitive. Finally, we use the combination of the ACT + *Planck* primary CMB, BAO from DESI, and our lensing measurements to revisit cosmological limits on the neutrino mass sum.

Data—We briefly describe the datasets and the external likelihoods used in this Letter.

CMB lensing spectra: We employ the CMB lensing spectrum measurements from ACT DR6 [19–21], *Planck* PR4 [32], and SPT-3G M2PM [22] with their respective survey footprints shown in Fig. 1.

The ACT DR6 lensing reconstruction [19–21] (red in Fig. 1) covers 23% of the sky and is signal-dominated on lensing scales with multipoles $L < 150$. The lensing spectrum is measured with a signal-to-noise ratio of 43 using a cross-correlation-based quadratic estimator that is insensitive to the modeling of instrumental noise [34,35]. In this analysis, we use the extended ACT DR6 multipole range of $40 \leq L \leq 1300$.

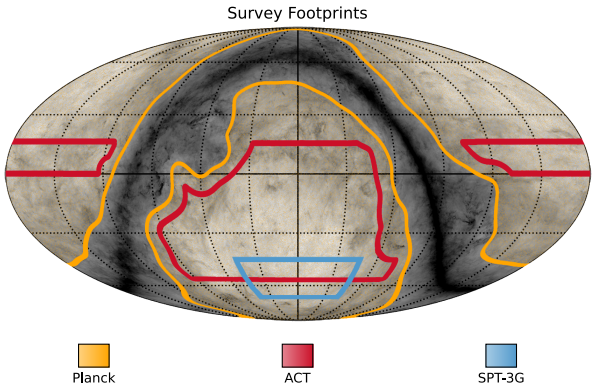

FIG. 1. Mollweide projection showing the sky coverage of ACT DR6 (red), *Planck* (orange), and SPT-3G M2PM (blue). ACT DR6 covers 23% of the sky, SPT-3G M2PM covers 3.5% and they overlap across 2.1% of the sky. *Planck* PR4 covers 67% of the sky. The gray scale background is a Galactic dust map from *Planck* [33].

The *Planck* PR4 lensing analysis [18] reconstructs lensing with the quadratic estimator using the reprocessed PR4 `NPIPE` CMB maps. It covers 67% of the sky (orange in Fig. 1) and is signal-dominated below $L \approx 70$. The lensing spectrum is measured with a signal-to-noise ratio of 42.

The SPT-3G M2PM lensing measurement [22] covers 3.5% of the sky (blue in Fig. 1). This analysis derives lensing information from CMB polarization maps using data collected with the SPT-3G camera during the 2019 and 2020 observing seasons. The analysis employs the marginal unbiased score expansion (MUSE) method [36,37] to infer CMB lensing and unlensed EE power spectra jointly. The lensing spectrum is signal-dominated for lensing multipoles $L < 240$ and is measured with a signal-to-noise ratio of 38.

BAO: We use the results from DESI data release 2 (DR2), consisting of BAO measured from more than 14×10^6 galaxies and quasars, as well as the DESI Lyman-α BAO [38,39] as our baseline baryonic acoustic oscillation combination. In the Supplemental Material [40], we show that using alternative BAO datasets yields consistent results with those obtained using DESI DR2 BAO.

Supernovae: For constraints on the Hubble constant that do not rely on the sound horizon, we include "uncalibrated" Type Ia supernovae from `Pantheon+` [52] as our baseline sample, although we also compare with `UNION3` [53] and `DESY5` [54]. Here, "uncalibrated" indicates that only the relation between the apparent magnitudes of Type Ia supernovae and their redshifts is employed—without anchoring their absolute magnitudes—and hence using these data cannot yield a determination of H_0.

Primary CMB: When constraining the neutrino mass sum, we add the primary CMB power spectrum measurement from *Planck* PR3 (including `high-`ℓ `TTTEEE, lowl T` and `SRoll2 EE` [55,56]) and ACT DR6 [15–17] (hereafter P-ACT), following the procedure in [16,17] to combine the two datasets. The comparisons of our measurements to the primary CMB are also done with respect to the P-ACT best-fit cosmology of [17] that we henceforth denote as CMB.

Likelihood—We build a Gaussian likelihood [57] from the CMB lensing bandpowers of ACT DR6 [19–21], *Planck* PR4 [18], and SPT-3G M2PM [22]:

$$-2\ln\mathcal{L} \propto \sum_{bb'} \begin{bmatrix} \Delta\hat{C}_b^{\kappa_A\kappa_A} \\ \Delta\hat{C}_b^{\kappa_P\kappa_P} \\ \Delta\hat{C}_b^{\kappa_S\kappa_S} \end{bmatrix} \mathbb{C}^{-1}_{bb'} \begin{bmatrix} \Delta\hat{C}_{b'}^{\kappa_A\kappa_A} \\ \Delta\hat{C}_{b'}^{\kappa_P\kappa_P} \\ \Delta\hat{C}_{b'}^{\kappa_S\kappa_S} \end{bmatrix}, \quad (1)$$

where $\Delta\hat{C}_b^{\kappa_i\kappa_i}$ $(i \in [A, P, S])$ are the residuals between observed and theory CMB lensing spectra for ACT DR6 (A), *Planck* PR4 (P), and SPT-3G M2PM (S). The covariance matrix $\mathbb{C}_{bb'}$ includes auto-covariances from simulations and cross covariances between experiments (see Supplemental Material [40]). Cross-correlations between ACT-SPT ($\lesssim$15%) and *Planck*-SPT ($\lesssim$10%) are small due to limited sky overlap and the different weighting of temperature versus polarization in the reconstructions.

We infer cosmological parameters using MCMC with Cobaya [58], evaluating fiducial lensing band powers with the `class_sz` emulator [59,60] for ΛCDM (with $\sum m_\nu = 60$ meV) and CAMB [61,62] for ΛCDM + Σm_ν models. Priors follow ACT DR6 [20] (Table I of the Supplemental Material [40]).

Results—

SPT-3G lensing-only constraints on structure growth: We present CMB lensing only constraints using SPT-3G M2PM. In [22], the amplitudes of CMB lensing and structure growth are derived simultaneously with CMB lensing and unlensed CMB EE bandpowers. In this Letter, since we aim to assess consistency across the three CMB lensing datasets, in the following we first report the lensing-only constraints from SPT-3G M2PM.

We estimate the lensing amplitude parameter $A_{\rm lens}^{\rm recon}$ from SPT-3G M2PM by fitting the SPT lensing bandpower measurements to a theory lensing power spectrum based on the best-fit ΛCDM model from CMB, allowing the amplitude of this lensing power spectrum to be a free parameter in our fit.

We find $A_{\rm lens}^{\rm recon} = 1.033 \pm 0.026$ (68% C.L.), in good agreement with the CMB ΛCDM prediction (i.e., $A_{\rm lens}^{\rm recon} = 1$), with a PTE χ^2 of 17% [63].

Analyzing only the SPT lensing band powers, we obtain a 1.9% constraint on structure growth given by

$$S_8^{\rm CMBL} = 0.827 \pm 0.016 \quad (68\%\,\text{C.L.}, \text{SPT-3G M2PM}). \quad (2)$$

TABLE I. Cosmological parameter measurements from the various lensing experiment combinations. We use A, P, and S as shorthands for CMB lensing with ACT DR6, *Planck* PR4 and SPT-3G M2PM, respectively.

Experiment	$S_8^{\rm lens}$	σ_8	Ω_m
A	0.830 ± 0.020	...	...
P	0.809 ± 0.022	...	...
S	0.827 ± 0.016	...	...
APS	$0.825^{+0.015}_{-0.013}$	...	...
A + BAO	0.826 ± 0.015	0.827 ± 0.014	0.298 ± 0.008
P + BAO	0.808 ± 0.018	0.811 ± 0.016	0.295 ± 0.008
S + BAO	0.830 ± 0.012	0.831 ± 0.012	0.298 ± 0.008
APS + BAO	0.829 ± 0.009	0.829 ± 0.009	0.300 ± 0.007

The high-precision small-scale lensing band powers from SPT-3G M2PM are highly complementary to those from ACT and *Planck*, which obtain higher precision on larger scales. The combination of all three datasets enables the tightest constraints on $S_8^{\rm CMBL}$ to date. With good agreement on $S_8^{\rm CMBL}$ between SPT-3G M2PM, ACT DR6, and *Planck* PR4 lensing (see Table I), we proceed in the next section to obtain results from the likelihood-level combination of the three CMB lensing measurements.

ACT + SPT + *Planck* (APS) joint constraints on structure growth: In Fig. 2, we show the individual lensing spectra from ACT DR6 (red), *Planck* PR4 (orange), and SPT-3G M2PM (blue). The joint lensing band powers, which are signal dominated at $L \lesssim 240$, are obtained by performing an amplitude fit on the bins between the three surveys against a theoretical lensing power spectrum predicted from the CMB best-fit ΛCDM model, in a similar way to a Bayesian linear regression [64].

The joint band powers have a lensing amplitude of

$$A_{\rm lens}^{\rm recon} = 1.025 \pm 0.017 \qquad (68\%\,\text{C.L., APS}), \quad (3)$$

with a signal-to-noise ratio of 61, making this the most precise CMB lensing power spectrum measurement to date and in excellent agreement with the primary CMB predictions within the ΛCDM model (we obtain similar $A_{\rm lens}^{\rm recon} = 1.010 \pm 0.016$ when comparing to the *Planck* best fit cosmology).

We measure $S_8^{\rm CMBL}$, which is the parameter combination best constrained by CMB lensing within the ΛCDM model, to 1.6%:

$$S_8^{\rm CMBL} = 0.825^{+0.015}_{-0.013} \qquad (68\%\,\text{C.L., APS}). \quad (4)$$

We can compare this result with the value expected from an extrapolation of the CMB data constraints within a ΛCDM cosmology, $S_8^{\rm CMBL} = 0.823 \pm 0.010$; this is fully consistent with our direct measurement [65].

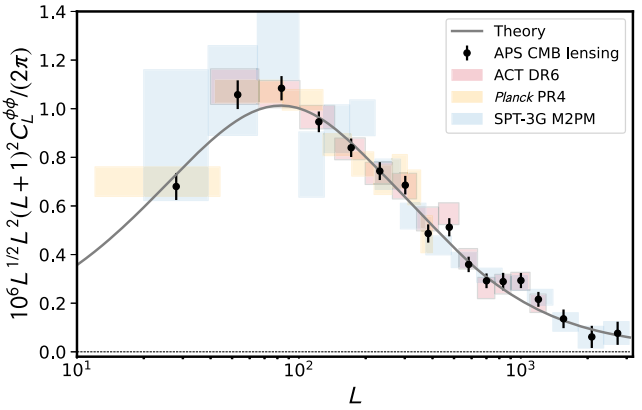

FIG. 2. We present the combined lensing band powers from the three surveys in black. In the background we show the *Planck* lensing band powers from PR4 NPIPE analysis in orange, the ACT DR6 lensing potential power spectrum band powers in red, and the lensing band powers from SPT-3G M2PM in blue. The gray line shows the theory prediction from the best-fit cosmology of the CMB likelihood. Note that we have applied an additional $L^{1/2}$ scaling over that usually used to display bandpowers to enhance visually the small scales.

These CMB lensing measurements provide information about a three-dimensional volume comprising the amplitude of matter fluctuations σ_8, the matter density Ω_m and the Hubble constant H_0. The inclusion of BAO data provides additional background information on the expansion history that helps break parameter degeneracies. This enables comparisons of σ_8 inferred from other probes such as cosmic shear and the primary CMB. With the addition of DESI BAO, we find

$$\sigma_8 = 0.829 \pm 0.009 \qquad (68\%\,\text{C.L., APS + BAO}). \quad (5)$$

This 1.1% measurement of σ_8 is consistent within 1.2σ with the value inferred from CMB, as can be seen in the marginalized constraints in Fig. 3. We note that this measurement is the most precise determination of σ_8 from either galaxy or CMB lensing to date. (See also Fig. 4 in the Supplemental Material [40].) We also achieve a competitive constraint on $S_8 \equiv \sigma_8(\Omega_m/0.3)^{0.5}$, the parameter combination best measured by cosmic shear, obtaining $S_8 = 0.828 \pm 0.012$.

Our lensing measurements are robust to the assumptions of the model—even in the presence of extensions that impact structure growth. The lensing constraints are only slightly weakened when we marginalize over neutrino mass; in this case we obtain $S_8^{\rm CMBL} = 0.818^{+0.017}_{-0.013}$, which is comparable to the CMB constraint of $S_8^{\rm CMBL} = 0.818 \pm 0.015$ under the same model with free $\sum m_\nu$. This robustness stems from the fact that the lensing measurement originates from relatively low redshifts and hence requires minimal extrapolation to $z = 0$ (where $S_8^{\rm CMBL}$ is evaluated). The same extrapolation effect and degeneracy breaking

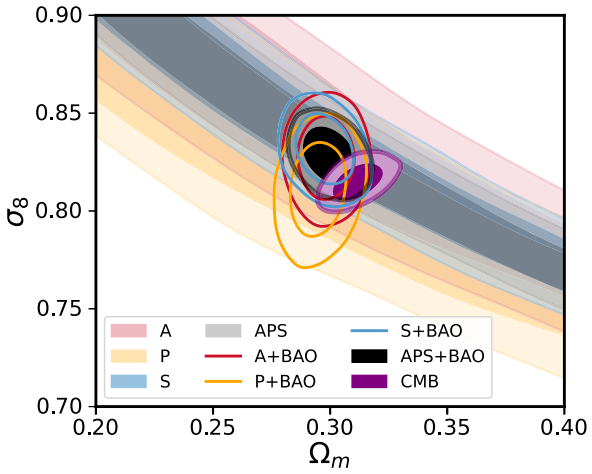

FIG. 3. Marginalized posteriors in the σ_8–Ω_m plane for ACT DR6 (red), *Planck* PR4 (orange), SPT-3G M2PM (blue), and APS (black) CMB lensing measurements. Filled contours in the background show lensing-only results, except for the black filled contour which represents APS + BAO. Nonfilled contours (outlined) show results when including BAO data, which further breaks degeneracies in structure growth. The purple contours show the CMB prediction for a ΛCDM model. Each dataset is shown with their 68% and 95% confidence limits.

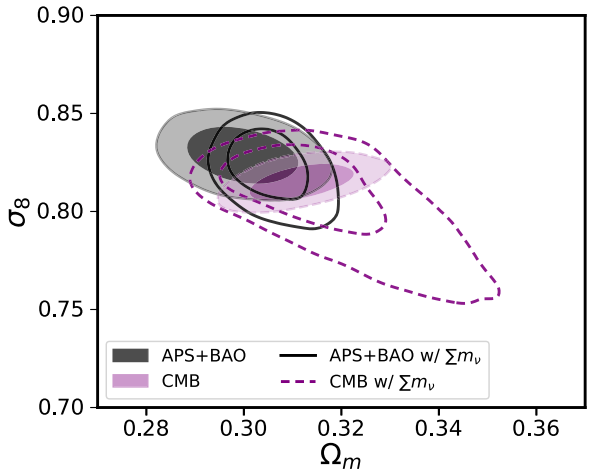

FIG. 4. Marginalized posteriors in the σ_8–Ω_m plane for APS CMB lensing + BAO (filled black) and the CMB prediction for a ΛCDM model (purple). Allowing the sum of the neutrino masses to vary results in the open contours. Each dataset is shown with their 68% and 95% confidence limits.

when including BAO explains how our σ_8 constraint with BAO, $\sigma_8 = 0.822 \pm 0.012$, becomes more competitive than the CMB extrapolation of $\sigma_8 = 0.808^{+0.029}_{-0.040}$ as shown in Fig. 4.

ACT + SPT + *Planck* joint constraints on the Hubble constant: We use our joint CMB lensing measurements to provide an independent constraint on the Hubble constant, H_0. While BAO observations, combined with a prior on $\Omega_b h^2$ [66], are sensitive to the expansion history, they exhibit an extended degeneracy between H_0 and Ω_m. In contrast, CMB lensing constrains a different degeneracy direction, making it complementary to BAO. Combining the baryon-drag-scale (r_d-)calibrated BAO with CMB lensing, we break parameter degeneracies and obtain tighter constraints on H_0 than from BAO-only measurements.

From the combination of the joint CMB lensing, galaxy BAO and the $\Omega_b h^2$ prior in Table I of the Supplemental Material [40], we obtain a 0.8% constraint on H_0:

$$H_0 = 68.77 \pm 0.53 \ \mathrm{km\,s^{-1}\,Mpc^{-1}} \times (68\%\,\mathrm{C.L.}, \mathrm{APS} + \mathrm{BAO}). \quad (6)$$

This result, shown in Fig. 5, is consistent with the results from the CMB ($H_0 = 67.62 \pm 0.50 \ \mathrm{km\,s^{-1}\,Mpc^{-1}}$) and in around 4σ tension with the SH0ES-inferred value of $73.17 \pm 0.86 \ \mathrm{km\,s^{-1}\,Mpc^{-1}}$ [67].

Most of the constraints on H_0 using BAO come exclusively from the knowledge of the sound horizon scale r_d. Following the method suggested by [68], we proceed to place sound-horizon-independent constraints on the Hubble constant; these constraints arise instead from the matter-radiation equality scale imprinted in the matter power spectrum to which CMB lensing is sensitive [69].

Combining our data with uncalibrated supernovae to break the degeneracy between H_0 and Ω_m, we find

$$H_0 = 66.4^{+2.5}_{-2.8} \ \mathrm{km\,s^{-1}\,Mpc^{-1}} \times (68\%\,\mathrm{C.L.}, \mathrm{APS} + \texttt{Pantheon+}). \quad (7)$$

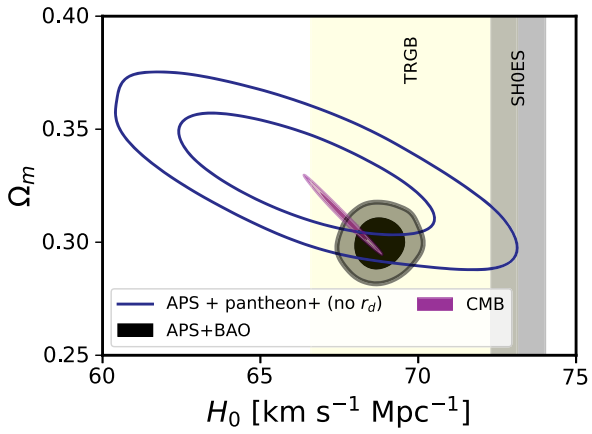

FIG. 5. Hubble constant measurements for the combination of CMB lensing and BAO are in filled black contours. The blue open contours show constraints on H_0 inferred from the matter-radiation equality scale as opposed to the sound-horizon scale. The H_0 measurements with CMB lensing are consistent with the low expansion rate inferred from the CMB in purple. We also show the 68% bands of the Cepheid-calibrated direct inference in gray and the TRGB-calibrated direct inference in yellow.

We also compute sound-horizon-free measurements using other supernova samples: $H_0 = 64.0^{+2.9}_{-3.5}$ km s^{-1} Mpc^{-1} with UNION3 and $H_0 = 64.2 \pm 2.4$ km s^{-1} Mpc^{-1} with DESY5; we note discussions in [70] and [71] regarding the DESY5 sample. Our sound-horizon-free measurements are consistent with the value of H_0 derived from the BAO + APS and primary CMB data. They are also in agreement with the direct distance ladder measurements calibrated using the tip of the red giant branch (TRGB) reported in [72] but differ from the SH0ES measurement by 2.5σ [67].

Neutrino mass: Massive neutrinos affect structure growth in the Universe after the neutrinos become nonrelativistic (e.g., [73]), leading to suppression of the matter power spectrum at the percent level. Since CMB lensing probes the distribution of mass in projection, it is a sensitive probe of the neutrino mass sum. Our baseline constraint uses CMB, BAO, and APS CMB lensing, resulting in

$$\Sigma m_\nu < 0.062\ \text{eV} \quad (95\%\,\text{C.L.}, \text{CMB} + \text{APS} + \text{BAO}). \quad (8)$$

The upper limit [74] is relatively stable to the primary CMB used (as also noted in [17]). Switching to *Planck* NPIPE CamSpec, the upper limit becomes $\sum m_\nu < 0.061$ eV (95% C.L.). While our results show a preference for a lower $\sum m_\nu$ compared to neutrino oscillation experiments, nominally disfavoring the inverted hierarchy at 3.3σ, alternative data combinations or modeling approaches can relax this upper limit, as we will discuss below.

Our neutrino mass constraints present only modest improvements over others in the literature, $\sum m_\nu < 0.082$ eV (95% C.L.) with CMB + AP lensing and DESI DR1 BAO [17] and $\sum m_\nu < 0.064$ eV (95% C.L.) in the case of *Planck* CMB + AP lensing and DESI DR2 BAO [38,39]. References [76,77] argue that such tight constraints arise partly from differences in the inferred matter density, with the matter density $\Omega_m h^2$ inferred from CMB + BAO close to (or even lower) than the mass densities of baryons and cold dark matter inferred from CMB data [76,77], leaving little room for the neutrino mass density. Reference [78] invokes a high lensing amplitude as a key factor in providing unexpectedly tight constraints on the neutrino mass sum.

Figure 6 summarizes some constraints on the neutrino mass sum based on different dataset choices. Replacing DESI DR2 BAO with BOSS BAO, one obtains

$$\Sigma m_\nu < 0.112\,\text{eV} \quad (95\%\,\text{C.L.}, \text{CMB} + \text{APS} + \text{BOSS BAO}). \quad (9)$$

Excluding BAO completely and instead using supernova measurements relaxes the bounds further and results in

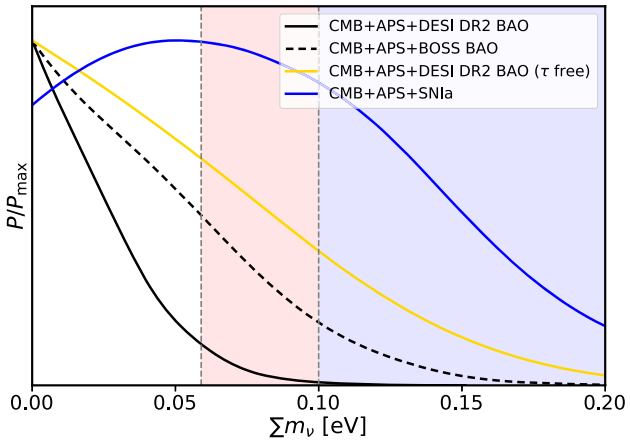

FIG. 6. 95% upper limits on the sum of the neutrino masses, $\sum m_\nu$, within the ΛCDM model. Reference [38] showed that this distribution is broadened when relaxing the assumption of the dark energy being a cosmological constant. The limits also become more relaxed when replacing DESI DR2 BAO with BOSS BAO (dashed black), Pantheon+ SNIa (blue) or when not relying on the optical depth τ by removing *Planck* low-ℓ EE (orange). The vertical dashed lines and shaded regions indicate the minimum allowed $\sum m_\nu$ values for the normal and inverted mass-ordering scenarios.

$$\Sigma m_\nu < 0.193\,\text{eV} \quad (95\%\,\text{C.L.}, \text{CMB} + \text{APS} + \text{Pantheon+}), \quad (10)$$

which is primarily driven by a higher Ω_m preferred by the Pantheon+ sample.

The neutrino mass sum is also degenerate with the reionization optical depth τ [78,79]. We can test the sensitivity of our constraints to our knowledge of reionization by excluding *Planck* low-ℓ EE, i.e., SRoll2, resulting in a relaxed upper bound of

$$\Sigma m_\nu < 0.150\,\text{eV} \quad (95\%\,\text{C.L.}, \text{CMB} + \text{APS} + \text{BAO}, \tau\,\text{free}). \quad (11)$$

So far, all neutrino mass constraints are derived within ΛCDM + $\sum m_\nu$. However, some models, such as ones that allow the dark energy equation of state to change with time [38,80], introduce parameters that are degenerate with $\Omega_m h^2$, opening up different ways to relax constraints on $\sum m_\nu$. We defer more exhaustive studies aimed at discerning the impact of data and model choices on constraints of the neutrino mass sum to future work.

Discussion—We have presented cosmological constraints from the first joint analysis of CMB lensing from ACT DR6, *Planck* PR4, and SPT-3G M2PM. Building on previous separate analyses of these datasets, we release a joint lensing likelihood and provide tight constraints on the amplitude of density fluctuations on mainly linear scales in

the redshift range $z \approx 0.9$–5. In the ΛCDM framework, we constrain S_8^{CMBL} to 1.6% and provide a 1.1% determination of σ_8 when combined with BAO.

The amplitudes of structure growth inferred from the three different experiments are fully consistent with each other, with each individual experiment constraining S_8^{CMBL} at around the 2% level. Our results are in excellent agreement with the model predictions from the ΛCDM fits to the CMB of P-ACT and reinforce the conclusions of [20–22,81] that structure growth follows ΛCDM expectations over a broad range of scales and redshifts.

In addition, using BAO, we provide a 0.8% constraint on the Hubble constant. We further measure H_0 independently of the sound horizon scale and BAO with 4% precision using uncalibrated supernovae. Both methods are in agreement with each other and in agreement with the constraints derived from the primary CMB.

Finally, with the assumption that the cosmological model is the $\Lambda\mathrm{CDM} + \sum m_\nu$ model, the combination of CMB, BAO and CMB lensing results in an upper bound on the neutrino mass sum $\Sigma m_\nu < 0.062$ eV (95% C.L.), compared with the physical prior $\Sigma m_\nu \geq 0.059$ eV from neutrino oscillation experiments [82,83]. Although our results are similar to previously reported constraints, understanding the origin of this tight neutrino mass constraint, including possible inconsistencies between different data types or specific assumptions about the cosmological model, remains important.

Combining multiple surveys probing the same observable has significant potential to improve the constraints of the cosmological parameters. We reached the highest signal-to-noise CMB lensing measurement by combining the individual measurements from ACT DR6, *Planck* PR4, and SPT-3G M2PM. This methodology not only highlights the current advantages of such synergistic approaches but also paves the way for even greater improvements as new CMB lensing data from ACT DR6+, SPT-3G [84], the Simons Observatory (SO) [85], CMB-S4 [86], and CMB-HD [87] become available.

Acknowledgments—W. L. K. W. acknowledges support from an Early Career Research Award of the Department of Energy and a Laboratory Directed Research and Development program as part of the Panofsky Fellowship program at the SLAC National Accelerator Laboratory. The SLAC authors acknowledge support by the Department of Energy, under Contract No. DE-AC02-76SF00515. I. A.-C. acknowledges support from Fundación Mauricio y Carlota Botton and the Cambridge International Trust. B. D. S. acknowledges support from the European Research Council (ERC) under the European Union's Horizon 2020 research and innovation programme (Grant Agreement No. 851274). B. D. S. further acknowledges support from an STFC Ernest Rutherford Fellowship. N. S. acknowledges support from DOE Award No. DE-SC0025309. A. C. acknowledges support from the STFC (Grants No. ST/W000977/1 and No. ST/X006387/1). J. D. acknowledges support from NSF Grant No. AST-2108126, from a Royal Society Wolfson Visiting Fellowship and from the Kavli Institute for Cosmology Cambridge and the Institute of Astronomy, Cambridge. O. D. acknowledges support from a SNSF Eccellenza Professorial Fellowship (No. 186879). C. S. acknowledges support from the Agencia Nacional de Investigación y Desarrollo (ANID) through Basal Project No. FB210003. K. M. acknowledges support from the National Research Foundation of South Africa. J. C. acknowledges support from a SNSF Eccellenza Professorial Fellowship (No. 186879). R. D. thanks ANID for Grants No. BASAL CATA FB210003, No. FONDEF ID21I10236, and No. QUIMAL240004. Support for ACT was through the U.S. National Science Foundation through Grants No. AST-0408698, No. AST-0965625, and No. AST-1440226 for the ACT project, as well as Grants No. PHY-0355328, No. PHY-0855887, and No. PHY-1214379. Funding was also provided by Princeton University, the University of Pennsylvania, and a Canada Foundation for Innovation (CFI) award to UBC. The development of multichroic detectors and lenses was supported by NASA Grants No. NNX13AE56G and No. NNX14AB58G. Detector research at NIST was supported by the NIST Innovations in Measurement Science program. ACT operated in the Parque Astronómico Atacama in northern Chile under the auspices of the Agencia Nacional de Investigación y Desarrollo (ANID). We thank the Republic of Chile for hosting ACT in the northern Atacama, and the local indigenous Licanantay communities whom we follow in observing and learning from the night sky. The South Pole Telescope program is supported by the National Science Foundation (NSF) through Grants No. OPP-1852617 and No. OPP-2332483. Partial support is also provided by the Kavli Institute of Cosmological Physics at the University of Chicago. Argonne National Laboratory's work was supported by the U.S. Department of Energy, Office of High Energy Physics, under Contract No. DE-AC02-06CH11357. Work at the Fermi National Accelerator Laboratory (Fermilab), a U.S. Department of Energy, Office of Science, Office of High Energy Physics HEP User Facility, is managed by Fermi Forward Discovery Group, LLC, acting under Contract No. 89243024CSC000002. Computations were performed on the Niagara supercomputer at the SciNet HPC Consortium. SciNet is funded by Innovation, Science and Economic Development Canada; the Digital Research Alliance of Canada; the Ontario Research Fund: Research Excellence; and the University of Toronto. This research also used resources of the National Energy Research Scientific Computing Center (NERSC), a DOE Office of Science User Facility supported by the Office of

Science of the U.S. Department of Energy under Contract No. DE-AC02-05CH11231.

Data availability—The data that support the findings of this article are openly available [88–90].

[1] K. M. Smith, O. Zahn, and O. Doré, Phys. Rev. D **76**, 043510 (2007).
[2] P. A. R. Ade *et al.* (Planck Collaboration), Astron. Astrophys. **571**, A17 (2014).
[3] P. A. R. Ade *et al.* (Planck Collaboration), Astron. Astrophys. **594**, A15 (2016).
[4] N. Aghanim *et al.* (Planck Collaboration), Astron. Astrophys. **641**, A8 (2020).
[5] S. Das *et al.*, Phys. Rev. Lett. **107**, 021301 (2011).
[6] B. D. Sherwin *et al.*, Phys. Rev. D **95**, 123529 (2017).
[7] A. van Engelen *et al.*, Astrophys. J. **756**, 142 (2012).
[8] K. T. Story *et al.*, Astrophys. J. **810**, 50 (2015).
[9] W. L. K. Wu *et al.*, Astrophys. J. **884**, 70 (2019).
[10] F. Bianchini *et al.* (SPT Collaboration), Astrophys. J. **888**, 119 (2020).
[11] Z. Pan *et al.* (SPT Collaboration), Phys. Rev. D **108**, 122005 (2023).
[12] For example, this can be seen from *Planck* [13,14] or from a combination of *Planck* large scales with ACT arcminute-scale measurements [15–17].
[13] N. Aghanim *et al.* (Planck Collaboration), Astron. Astrophys. **641**, A6 (2020); **652**, C4(E) (2021).
[14] E. Rosenberg, S. Gratton, and G. Efstathiou, Mon. Not. R. Astron. Soc. **517**, 4620 (2022).
[15] S. Naess, Y. Guan, A. J. Duivenvoorden, M. Hasselfield, Y. Wang *et al.*, J. Cosmol. Astropart. Phys. 11 (2025) 061.
[16] T. Louis, A. L. Posta, Z. Atkins, H. T. Jense *et al.*, J. Cosmol. Astropart. Phys. 11 (2025) 062.
[17] E. Calabrese, J. C. Hill, H. T. Jense, A. L. Posta *et al.*, J. Cosmol. Astropart. Phys. 11 (2025) 063.
[18] Y. Akrami *et al.* (Planck Collaboration), Astron. Astrophys. **643**, A42 (2020).
[19] F. J. Qu *et al.* (ACT Collaboration), Astrophys. J. **962**, 112 (2024).
[20] M. S. Madhavacheril *et al.* (ACT Collaboration), Astrophys. J. **962**, 113 (2024).
[21] N. MacCrann *et al.*, Astrophys. J. **966**, 138 (2024).
[22] F. Ge *et al.* (SPT-3G Collaboration), Phys. Rev. D **111**, 083534 (2025).
[23] A. Amon *et al.* (DES Collaboration), Phys. Rev. D **105**, 023514 (2022).
[24] L. F. Secco *et al.* (DES Collaboration), Phys. Rev. D **105**, 023515 (2022).
[25] T. M. C. Abbott *et al.* (DES Collaboration), Phys. Rev. D **105**, 023520 (2022).
[26] E. P. Longley *et al.* (LSST Dark Energy Science Collaboration), Mon. Not. R. Astron. Soc. **520**, 5016 (2023).
[27] M. Asgari *et al.* (KiDS Collaboration), Astron. Astrophys. **645**, A104 (2021).
[28] C. Heymans *et al.*, Astron. Astrophys. **646**, A140 (2021).
[29] X. Li *et al.*, Phys. Rev. D **108**, 123518 (2023).
[30] R. Dalal *et al.*, Phys. Rev. D **108**, 123519 (2023).
[31] A. H. Wright *et al.*, Astron. Astrophys. **703**, A158 (2025).
[32] J. Carron, M. Mirmelstein, and A. Lewis, J. Cosmol. Astropart. Phys. 09 (2022) 039.
[33] R. Adam, P. A. R. Ade, N. Aghanim, M. I. R. Alves, M. Arnaud, M. Ashdown, J. Aumont, C. Baccigalupi, A. J. Banday *et al.* (Planck Collaboration), Astron. Astrophys. **594**, A10 (2016).
[34] M. S. Madhavacheril, K. M. Smith, B. D. Sherwin, and S. Naess, J. Cosmol. Astropart. Phys. 05 (2021) 028.
[35] Z. Atkins *et al.*, J. Cosmol. Astropart. Phys. 11 (2023) 073.
[36] M. Millea and U. c. v. Seljak, Phys. Rev. D **105**, 103531 (2022).
[37] M. Millea, arXiv:2209.10512.
[38] Abdul-Karim *et al.* (DESI Collaboration), Phys. Rev. D **112**, 083514 (2025).
[39] Abdul-Karim *et al.* (DESI Collaboration), Phys. Rev. D **112**, 083515 (2025).
[40] See Supplemental Material at http://link.aps.org/supplemental/10.1103/k5yr-3h6d for detailed derivations of covariance matrices, systematic error analyses, and additional validation tests, which includes Refs. [41–51].
[41] A. Gelman and D. B. Rubin, Stat. Sci. **7**, 457 (1992).
[42] A. Mead, C. Heymans, L. Lombriser, J. Peacock, O. Steele, and H. Winther, Mon. Not. R. Astron. Soc. **459**, 1468 (2016).
[43] N. Aghanim *et al.* (Planck Collaboration), Astron. Astrophys. **641**, A8 (2020).
[44] V. Mossa *et al.*, Nature (London) **587**, 210 (2020).
[45] D. Hanson, A. Challinor, G. Efstathiou, and P. Bielewicz, Phys. Rev. D **83**, 043005 (2011).
[46] M. M. Schmittfull, A. Challinor, D. Hanson, and A. Lewis, Phys. Rev. D **88**, 063012 (2013).
[47] F. Beutler, C. Blake, M. Colless, D. H. Jones, L. Staveley-Smith, L. Campbell, Q. Parker, W. Saunders, and F. Watson, Mon. Not. R. Astron. Soc. **416**, 3017 (2011).
[48] A. J. Ross, L. Samushia, C. Howlett, W. J. Percival, A. Burden, and M. Manera, Mon. Not. R. Astron. Soc. **449**, 835 (2015).
[49] S. Alam *et al.*, Mon. Not. R. Astron. Soc. **470**, 2617 (2017).
[50] S. Alam *et al.*, Phys. Rev. D **103**, 083533 (2021).
[51] D. C. *et al.*, J. Cosmol. Astropart. Phys. 02 (2025) 021.
[52] D. Brout *et al.*, Astrophys. J. **938**, 110 (2022).
[53] D. Rubin, G. Aldering, M. Betoule, A. Fruchter, X. Huang, A. G. Kim, C. Lidman, E. Linder, S. Perlmutter, P. Ruiz-Lapuente, and N. Suzuki, Astrophys. J. **986**, 231 (2025).
[54] T. M. C. Abbott *et al.* (DES Collaboration), Astrophys. J. Lett. **973**, L14 (2024).
[55] N. Aghanim *et al.* (Planck Collaboration), Astron. Astrophys. **641**, A5 (2020).
[56] J. M. Delouis, L. Pagano, S. Mottet, J. L. Puget, and L. Vibert, Astron. Astrophys. **629**, A38 (2019).
[57] The likelihood is publicly available at https://github.com/qujia7/spt_act_likelihood.
[58] J. Torrado and A. Lewis, J. Cosmol. Astropart. Phys. 05 (2021) 057.
[59] B. Bolliet, B. Comis, E. Komatsu, and J. F. Macías-Pérez, Mon. Not. R. Astron. Soc. **477**, 4957 (2018).
[60] B. Bolliet *et al.*, EPJ Web Conf. **293**, 00008 (2024).
[61] A. Lewis, A. Challinor, and A. Lasenby, Astrophys. J. **538**, 473 (2000).

[62] C. Howlett, A. Lewis, A. Hall, and A. Challinor, J. Cosmol. Astropart. Phys. 04 (2012) 027.
[63] We note that these results are consistent with the one combining *Planck* primary CMB and SPT-3G M2PM lensing in [22].
[64] The joint band powers are only used to calculate the lensing amplitude, the SNR and for the visual representation in Fig. 2. We use Eq. (1) for all the parameter constraints in the rest of this Letter.
[65] Here the neutrino mass sum is fixed to 60 meV which is close to the minimum mass allowed in the normal hierarchy by constraints from neutrino oscillations. We later explore the impact of marginalizing over the neutrino mass sum.
[66] BBN is required to calibrate the BAO and break the degeneracy between r_d and H_0.
[67] L. Breuval, A. G. Riess, S. Casertano, W. Yuan, L. M. Macri, M. Romaniello, Y. S. Murakami, D. Scolnic, G. S. Anand, and I. Soszyński, Astrophys. J. **973**, 30 (2024).
[68] E. J. Baxter and B. D. Sherwin, Mon. Not. R. Astron. Soc. **501**, 1823 (2020).
[69] Lensing is sensitive to the broadband shape of the matter power spectrum, with the location of the peak determining the scale of the matter-radiation equality.
[70] G. Efstathiou, Mon. Not. R. Astron. Soc. **538**, 875 (2025).
[71] M. Vincenzi *et al.* (DES Collaboration), Mon. Not. R. Astron. Soc. **541**, 2585 (2025).
[72] W. L. Freedman, B. F. Madore, I. S. Jang, T. J. Hoyt, A. J. Lee, and K. A. Owens, Astrophys. J. **985**, 203 (2025).
[73] J. Lesgourgues and S. Pastor, Adv. High Energy Phys. **2012**, 1 (2012).
[74] We model neutrinos as a combination of three degenerate equal-mass particles following [73,75] consistent with recent cosmological analyses [20,38,39]. We note that adopting an alternative prescription of one massive and two massless neutrinos, as used by [22], yields $\Sigma m_\nu < 0.053$ eV (95% C.L.)using the same data combination as above.
[75] E. Di Valentino *et al.*, J. Cosmol. Astropart. Phys. 04 (2018) 017.
[76] M. Loverde and Z. J. Weiner, J. Cosmol. Astropart. Phys. 12 (2024) 048.
[77] G. P. Lynch and L. Knox, Phys. Rev. D **112**, 083543 (2025).
[78] D. Green and J. Meyers, Phys. Rev. D **111**, 083507 (2025).
[79] N. Craig, D. Green, J. Meyers, and S. Rajendran, J. High Energy Phys. 09 (2024) 097.
[80] C. Garcia-Quintero *et al.*, Phys. Rev. D **112**, 083529 (2025).
[81] G. S. Farren, A. Krolewski, F. J. Qu, S. Ferraro, E. Calabrese, J. Dunkley, C. E. Villagra, J. C. Hill, J. Kim, M. S. Madhavacheril, K. Moodley, L. A. Page, B. Partridge, N. Sehgal, B. D. Sherwin, C. Sifón, S. T. Staggs, A. V. Engelen, and E. J. Wollack, Phys. Rev. D **111**, 083516 (2025).
[82] I. Esteban, M. C. Gonzalez-Garcia, A. Hernandez-Cabezudo, M. Maltoni, and T. Schwetz, J. High Energy Phys. 01 (2019) 106.
[83] S. Navas *et al.* (Particle Data Group Collaboration), Phys. Rev. D **110**, 030001 (2024).
[84] K. Prabhu, S. Raghunathan, M. Millea, G. Lynch *et al.*, Astrophys. J. **973**, 4 (2024).
[85] P. Ade, J. Aguirre, Z. Ahmed, S. Aiola, A. Ali, D. Alonso, M. A. Alvarez, K. Arnold, P. Ashton, J. Austermann *et al.*, J. Cosmol. Astropart. Phys. 02 (2019) 056.
[86] K. Abazajian *et al.* (CMB-S4 Collaboration), arXiv:1907.04473.
[87] S. Aiola *et al.* (CMB-HD Collaboration), arXiv:2203.05728.
[88] ACT, Planck, and SPT Collaborations, MCMC chains for joint ACT, Planck, and SPT lensing analysis, https://portal.nersc.gov/cfs/act/aps_lensing/chains/ (2024), data available at NERSC.
[89] F. J. Qu *et al.*, Likelihood code for SPT-ACT joint lensing analysis, https://github.com/qujia7/spt_act_likelihood (2024), code available on GitHub.
[90] ACT and SPT Collaborations, NASA/GSFC LAMBDA (Legacy Archive for Microwave Background Data Analysis), v1.0 (Likelihood Code v1), https://lambda.gsfc.nasa.gov/product/act/actadv_act_spt_joint_prod_get.html (2025).